Computers in Biology and Medicine 114 (2019) 103438

Contents lists available at ScienceDirect

Computers in Biology and Medicine

journal homepage: http://www.elsevier.com/locate/compbiomed

Automatic segmentation of the uterus on MRI using a convolutional neural network

Yasuhisa Kurata [a,b], Mizuho Nishio [a,c,*], Aki Kido [a], Koji Fujimoto [d], Masahiro Yakami [a,c], Hiroyoshi Isoda [a,c], Kaori Togashi [a]

[a] *Department of Diagnostic Imaging and Nuclear Medicine, Kyoto University Graduate School of Medicine, 54 Kawahara-cho, Shogoin, Sakyoku, Kyoto, 606-8507, Japan*
[b] *Department of Diagnostic Radiology, Kobe City Medical Center General Hospital, 2-1-1, Minatojimaminamimachi, Chuo-ku, Kobe, Hyogo, 650-0047, Japan*
[c] *Preemptive Medicine and Lifestyle-Related Disease Research Center, Kyoto University Hospital, 54 Kawahara-cho, Shogoin, Sakyoku, Kyoto, 606-8507, Japan*
[d] *Human Brain Research Center Kyoto University Graduate School of Medicine, 54 Kawahara-cho, Shogoin, Sakyoku, Kyoto, 606-8507, Japan*

ARTICLE INFO

Keywords:
Uterus
Segmentation
Convolutional neural network
CNN
U-net

ABSTRACT

Background: This study was performed to evaluate the clinical feasibility of a U-net for fully automatic uterine segmentation on MRI by using images of major uterine disorders.
Methods: This study included 122 female patients (14 with uterine endometrial cancer, 15 with uterine cervical cancer, and 55 with uterine leiomyoma). U-net architecture optimized for our research was used for automatic segmentation. Three-fold cross-validation was performed for validation. The results of manual segmentation of the uterus by a radiologist on T2-weighted sagittal images were used as the gold standard. Dice similarity coefficient (DSC) and mean absolute distance (MAD) were used for quantitative evaluation of the automatic segmentation. Visual evaluation using a 4-point scale was performed by two radiologists. DSC, MAD, and the score of the visual evaluation were compared between uteruses with and without uterine disorders.
Results: The mean DSC of our model for all patients was 0.82. The mean DSCs for patients with and without uterine disorders were 0.84 and 0.78, respectively ($p = 0.19$). The mean MADs for patients with and without uterine disorders were 18.5 and 21.4 [pixels], respectively ($p = 0.39$). The scores of the visual evaluation were not significantly different between uteruses with and without uterine disorders.
Conclusions: Fully automatic uterine segmentation with our modified U-net was clinically feasible. The performance of the segmentation of our model was not influenced by the presence of uterine disorders.

1. Introduction

MRI is widely used for various purposes such as the differential diagnosis of benign and malignant gynecologic disorders, as well as clinical staging of malignant tumors, in modern clinical practice. Recently, deep learning through convolutional neural networks (CNNs) has gathered attention in various fields, including image recognition [1]. CNN is a type of neural network that is commonly used for efficient image recognition and further image analysis [2]. Notably, CNN enables automatic image feature extraction, whereas conventional machine-learning techniques require customized feature extraction [3]. Several studies regarding the application of deep learning to medical images have been reported in areas such as lesion detection, classification, and segmentation [4–10]. There have been several reports of image texture analysis for gynecologic diseases [11–13]. To the best of our knowledge, there are no report of image analysis using deep learning for gynecologic diseases on MRI.

For the analysis of medical images via deep learning, including radiomic or radiogenomic approaches, the segmentation of the object is often essential. Manual segmentation by experienced clinicians, such as radiologists, is important; however, it is laborious and time-consuming, and may be subjective. Another approach for image segmentation, a fully convolutional neural network known as U-net, has recently shown promising results [14]. U-net has been applied for the automatic segmentation of some organs, including breast, prostate, spinal cord, vessel wall, and knee joint on MRI [10,15–18]. U-net is an end-to-end encoder-decoder network that was originally designed for biomedical image segmentation. The original U-net architecture comprises a contracting

---

* Corresponding author. 54 Kawahara-cho, Shogoin, Sakyoku, Kyoto, 606-8507, Japan.
E-mail address: nishio.mizuho.3e@kyoto-u.jp (M. Nishio).

https://doi.org/10.1016/j.compbiomed.2019.103438
Received 10 May 2019; Received in revised form 20 August 2019; Accepted 4 September 2019

path for encoding features using convolution and max pooling, as well as a symmetrical expansive path for localization. The expansive path involves upsampling and concatenation, followed by convolution operation. Upsampling operators enable the network to propagate context information to higher resolution layers. As a network structure for localization, high-resolution features from the contracting path are concatenated with the output of the upsampling.

T2-weighted images are important for the diagnosis of gynecologic diseases, because these images clearly represent the anatomical structure of the uterus and reveal the presence of uterine diseases, such as uterine leiomyoma, cervical cancer, and endometrial cancer. Thus, we aim to perform automatic uterine segmentation of T2-weighted MR images. Automatic uterine segmentation could be useful for automatic segmentation of uterine diseases by using a cascaded fully convolutional neural network, which enables sequential segmentation of uterus and uterine lesions [6]. In addition, automatic uterine segmentation could be utilized for the staging of uterine endometrial cancer. Accurate uterine segmentation would enable the diagnosis of the extent of tumor invasion to the uterine myometrium. Additionally, our research is focused on whether uterine diseases affect the difficulty involved in automatic segmentation. As radiologists, we consider it to be more difficult to segment the uterus in some disorders, because the diseased uterus can vary in shape and intensity on MRI.

The purpose of this study was to evaluate the clinical feasibility of fully automatic uterine segmentation on MRI by using images of major uterine disorders. We applied U-net and optimized some hyperparameters for automatic segmentation.

2. Materials and methods

Our institutional review board approved this single-center retrospective study. The requirement for written informed consent was waived by the review board.

2.1. Patient population

Patients who underwent uterine MRI in our hospital for various gynecologic disorders, between January 1, 2016 and March 15, 2016, were included in this study. Pregnant patients were excluded because the size and shape of the pregnant uterus is considerably different from that of a nonpregnant uterus. Finally, 122 female patients (mean age: 49.1 years, standard deviation [SD]: 15.2 years) were included in this study. Among these patients, 14 had uterine endometrial cancer, 15 had uterine cervical cancer, and 55 had uterine leiomyoma. Some patients with endometrial cancer or cervical cancer also had leiomyoma. Fifty patients had no uterine disease.

2.2. MRI protocol

MRI was performed using a 1.5-T or 3.0-T unit (Avanto, Skyra, Prisma; Siemens Health Care, Erlagen, Germany) using a phased-array coil. Before MR examination, 20 mg of butyl scopolamine (Buscopan; Nippon Boehringer Ingelheim, Tokyo, Japan) was administered intramuscularly to each patient. Only sagittal fast spin echo T2-weighted imaging was used in this study. The acquisition parameters were as follows: repetition time/echo time [TR/TE], 4000–5800/72–125 msec; slice thickness, 4–5 mm; matrix size, 384-1024 × 308–1024; flip angle, 150; and bandwidth, 320 Hz/pixel.

2.3. Image preprocessing

A board-certified radiologist with 10 years of experience specializing in gynecologic imaging manually segmented each uterus, including lesions (e.g., uterine tumor), on each slice of sagittal T2-weighted imaging using 3DSlicer (https://www.slicer.org/) [19]. These regions of interest were used as the gold standard for uterine segmentation. All MR images were reformatted to 512 × 512 pixels; the MR signal intensity (SI) of each image was normalized based on the following equation (1):

$$nSI = \frac{(SI - mean\_of\_SI)}{(3 \times SD\_of\_SI)} \tag{1}$$

where *nSI* is normalized SI, *mean_of_SI* is the mean SI of the image, and *SD_of_SI* is the SD of the SI of the image [20].

For input data, three consecutive slices of MR images, including slices without uterus, were used as one set. From the 122 included patients, 3350 sets (three consecutive image slices each) were obtained. Data augmentation was applied during the training phase and 20000 sets of slices were used as one epoch. Data augmentation comprised vertical and horizontal flip, ±20° rotation, ±10% x-axis shift, ±10% y-axis shift, and scaling from 85 to 115%, and shear mapping of 17°. The output was the predicted segmentation of the uterus, resulting in three consecutive images of 512 × 512 pixels. For comparison, we evaluated the performance of our final model using single-slice of MR images as input data.

2.4. Neural network architecture

The original U-net architecture is presented in Fig. 1 [14]. U-net architecture comprises a contracting path and an expansive path, which combine to generate the U-shaped architecture. Our final modified U-net architecture employed in this study is shown in Fig. 2. In each layer of the contracting path, 3 × 3 convolutions, batch normalization, leaky rectified linear unit (leaky-ReLU), and dropout layer are repeated twice, followed by a 2 × 2 max pooling operation with stride 2 for downsampling. In the expansive path, each layer consists of upsampling of the feature map by a 2 × 2 convolution and concatenation with the feature map from the contracting path, followed by two 3 × 3 convolutions, batch normalization, leaky-ReLU, and dropout layers (as in the contracting path). We employed batch size of 1, 5, and 15. We implemented 4, 6, and 8 downsampling and upsampling layers. Dice loss function was used as the cost function [21]. Three-fold cross-validation at the patient level was performed with two-thirds of the data used for training and one-third of the data used for validation. Our model was built by Keras (ver. 2.0.8) and Tensorflow (ver. 1.8.0), and the model was trained on a Tesla V100 graphic card (NVIDIA, Santa Clara, CA, USA).

2.5. Quantitative evaluation of automatic segmentation of the uterus

Regarding area-based metrics, the Dice similarity coefficient (DSC) was used to compare the performance of our model between patients with and without each gynecological disorder. For example, DSC of patients with uterine endometrial cancer was compared to that of patients without uterine endometrial cancer (patients in both groups might have uterine leiomyoma). In addition, DSC of patients with any of the diseases was compared to DSC of patients without any disease. DSC was calculated as follows (2):

$$\frac{2|T \cap P|}{(|T| + |P|)} \tag{2}$$

where T is the true manual segmentation map and P is the predicted segmentation map [22]. DSC of 0 indicates no overlap, whereas DSC of 1 indicates perfect overlap between two binary masks. Before calculating DSC between the gold standard and the automatic segmentation results by our U-net, post-processing was performed for the segmentation results. First, the predicted segmentation map (output of the CNN) was arranged in a sequential manner and binarized using the threshold value of 0.5. Next, the largest connected component was extracted three-dimensionally from the binarized results, and the results of extraction were used to calculate DSC. The same post-processing was performed before visual evaluation by the radiologists (described in the next section).

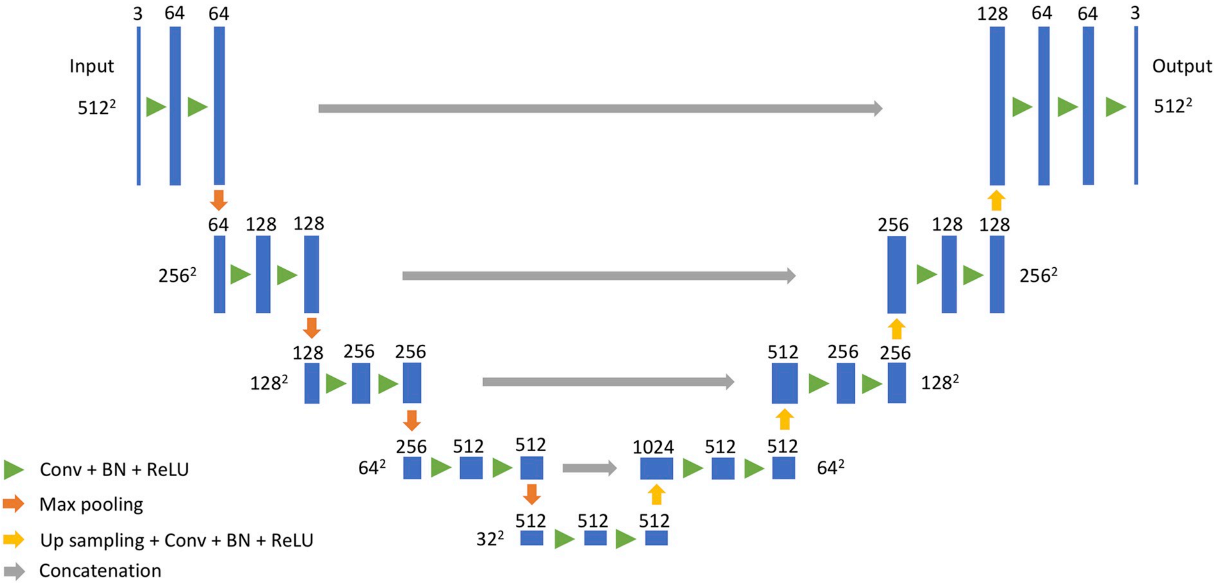

Fig. 1. Original U-net architecture
Conv: convolution
BN: batch normalization
ReLU: rectified linear unit.

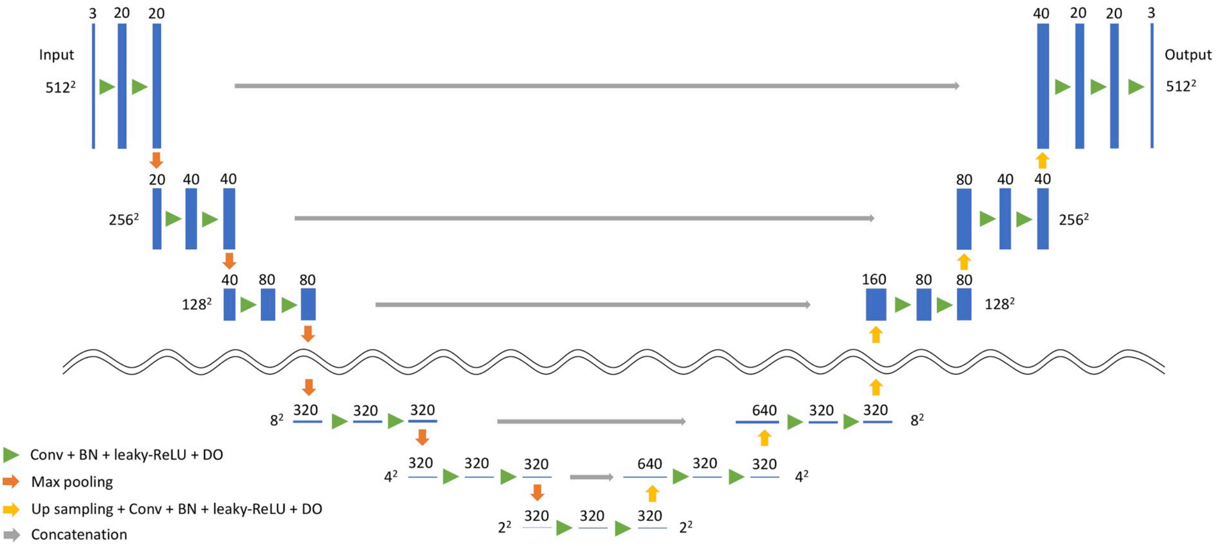

Fig. 2. Our U-net architecture.
Conv: convolution
BN: batch normalization
ReLU: rectified linear unit
DO: dropout.

Regarding distance-based metrics, mean absolute distance (MAD) was used to evaluate the performance of our model. MADs of patients with and without uterine diseases were compared. The minimum distance between a point p (automatically segmented points) and the gold standard (manually segmented contour) was defined as follows (3):

$$d_{min}(p,\ C)\ = \min_{q \in C} \|p - q\ \| \tag{3}$$

where $d_{\min}$ denotes the Euclidean distance between p and any point on the contour C.

The MAD between C_A (points on the automatically segmented contour) and C_M (points on the manually segmented contour) was calculated as follows (4):

$$MAD\ = \frac{1}{|C_A|}\sum_{p \in C_A} d_{min}(p,\ C_M) \tag{4}$$

where $|C_A|$ denotes the number of points in the set C_A.

2.6. Visual evaluation of the automatic segmentation of the uterus

Two board-certified radiologists with 21 years (Reader A) and 13 years (Reader B) of experience visually evaluated the quality of the automatic uterine segmentation by our model, using a 4-point scale (4 = excellent: > 90% of the uterus was correctly segmented and organs outside the uterus, such as ovaries and small intestine, were not included in the segmented area; 3 = good: > 80% of the uterus was correctly segmented and organs outside the uterus were included in fewer than three slices of MRI; 2 = fair: > 60% of the uterus was correctly segmented and organs outside the uterus were included in three or more slices of MRI; 1 = poor: ≤ 60% of the uterus was segmented correctly). The scores were also compared between uteruses with and without uterine disorders.

2.7. Statistical analysis

The Mann-Whitney *U* test was used to compare the DSC and MAD between patients with and without each uterine disease. Fisher's two-sided exact test was adopted to compare the results of visual evaluation between uteruses with and without uterine disorders. The degree of interobserver agreement was calculated using weighted kappa statistics. A kappa value of 0.21–0.40 was defined as fair agreement, 0.41–0.60 as moderate agreement, 0.61–0.80 as substantial agreement, and 0.81–1.00 as excellent agreement [23]. Statistical analyses were performed using a commercially available software (JMP version 12.2.0; SAS Institute Inc., Cary, NC, USA) and R software (version 3.3.2; The R Foundation for Statistical Computing, Vienna, Austria). A *P*-value less than 0.05 was considered to be statistically significant.

3. Results

The Dice losses of our network over three-fold cross validation with batch sizes of 1, 5 and 15 were 0.755, 0.257, and 0.180, respectively. Thus, we adopted a batch size of 15 in our model. The Dice losses with 4, 6, and 8 of downsampling and upsampling layers were 0.183, 0.183 and 0.180, respectively. Thus, we adopted 8 layers in our final model. The Dice loss obtained with three consecutive slices of MR images and single-slice of images as input data were 0.196 and 0.180, respectively. The Dice loss of the original U-net was 0.295. The mean DSCs and MADs with 95% confidence interval of our model for all patients are summarized in Tables 1 and 2, respectively. Regarding these analyses, there were no statistically significant differences between uteruses with and without lesions.

Regarding visual evaluation, reader A scored 4 for 38 patients (31%), 3 for 31 patients (25%), 2 for 44 patients (36%), and 1 for 9 patients (7%). Reader B scored 4 for 49 patients (40%), 3 for 23 patients (19%), 2 for 44 patients (36%), and 1 for 6 patients (5%). Interobserver agreement was substantial (kappa = 0.78). Between patients with and without uterine endometrial cancer, uterine cervical cancer, uterine leiomyoma and any disease, there were no statistically significant differences (p = 0.48, 0.27, 0.62, and 0.86 for reader A; p = 0.91, 0.12, 0.60, and 0.94 for reader B, respectively).

Representative results of automatic segmentation of uterus are shown in Fig. 3. In successful cases, the uterus was well-segmented automatically, despite the presence of some disorders (Fig. 3b). In unsuccessful cases, structures adjacent to the uterus (e.g., small intestines and ovaries) were included in the segmented area (Fig. 3c).

4. Discussion

This study demonstrated that automatic uterine segmentation was feasible using a CNN, regardless of the presence of major uterine disorders. In the future, automatic segmentation of the uterus could be further combined with automatic lesion detection or computer-aided

Table 1
Average value of the Dice similarity coefficient of our model for uterine segmentation with and without uterine disorders.

	+	-	p-value
endometria cancer	0.86 [0.82, 0.90]	0.81 [0.78, 0.84]	0.60
cervical cancer	0.79 [0.72, 0.85]	0.82 [0.79, 0.85]	0.10
leiomyoma	0.85 [0.82, 0.87]	0.79 [0.75, 0.83]	0.09
Any disease	0.84 [0.82, 0.84]	0.78 [0.72, 0.83]	0.19

Table 2
Average value of the mean absolute distance [pixels] of our model for uterine segmentation with and without uterine disorders.

	+	-	p-value
endometria cancer	16.4 [9.90, 22.9]	20.1 [14.2, 25.9]	0.67
cervical cancer	24.3 [12.6, 35.9]	19.0 [13.2, 24.8]	0.23
leiomyoma	18.9 [13.3, 24.6]	20.2 [11.8, 28.7]	0.25
Any disease	18.5 [13.8, 23.1]	21.4 [10.3, 32.5]	0.39

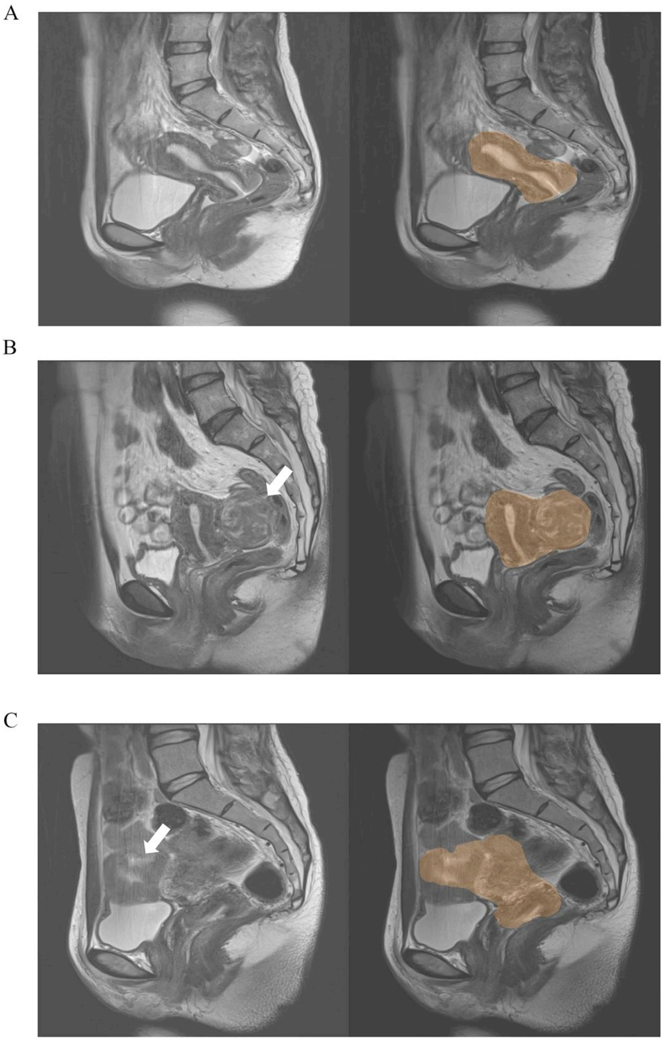

Fig. 3. Representative result of automatic segmentation of the uterus.
Left: sagittal T2-weighted MR image,
Right: fusion image of the sagittal T2-weighted MR image and the results of automatic segmentation of the uterus by our model.
a: Normal uterus
The result of automatic segmentation was good. Dice similarity coefficient was 0.95 and the score of visual evaluation was 4 for both readers.
b: Uterus with subserosal leiomyoma
The result of automatic segmentation was good, including subserosal leiomyoma on the posterior myometrium (Left, arrow). Dice similarity coefficient was 0.87 and the score of visual evaluation was 4 for both readers.
c: Normal uterus
Small intestine around uterus (Left, arrow) was included in the area of automatic segmentation. Dice similarity coefficient was 0.68 and the score of visual evaluation was 2 for both readers.

diagnosis of uterine diseases by deep learning methods. Moreover, automatic segmentation of other organs could be performed in a similar manner as that used in the present study.

To the best of our knowledge, there have been few studies regarding automatic segmentation of the uterus on MRI. Before the development of U-net, Fallahi et al. and Militello et al. reported automatic uterine segmentation in patients with uterine leiomyoma [24,25]. They used the Fuzzy C-means algorithm and morphological operations for automatic segmentation; the DSCs of their studies were 0.80 and 0.88, respectively. Compared with our study, the numbers of patients were limited in their studies (122 in our study vs. 10 in Fallahi's study and 15 in Militello's study); our study also included patients with uterine diseases other than uterine leiomyoma. This could increase the versatility and robustness of our model concerning automatic uterine segmentation. In addition, visual assessment by radiologists was not performed in the prior studies. One of the strengths of our study is that we validated the performance of our segmentation system in a clinical context. There have been a few studies regarding automatic segmentation of uterine leiomyoma [25–28]. While we focused on automatic segmentation of the uterus, our methodology can also be applied to automatic segmentation of uterine leiomyoma. By constructing region of interest on uterine leiomyomas for the reference standard, and using our U-net architecture, automatic segmentation of uterine leiomyoma could be achieved. Automatic segmentation of uterus could also be utilized for uterine lesions, including leiomyomas, by applying cascaded segmentation. Although manual segmentation is frequently performed to evaluate treatment outcomes in uterine leiomyoma, manual segmentation is operator-dependent and laborious [28]. Our segmentation system might be useful in evaluating treatment outcomes of uterine leiomyoma.

A recent report of automatic segmentation of prostate using U-net on T2-weighted MR images demonstrated promising results; the mean DSC was 0.927 for the total prostate gland and 0.793 for the total peripheral zone [15]. Although the mean DSC of our model was relatively high (0.82), it did not match that of the result of automatic segmentation of the prostate. This could be because the uterus is anatomically more complex than the prostate. Notably, the uterus sometimes bends forward or backward; in subserosal uterine leiomyoma, the uterus outline could be changed dramatically. Furthermore, there are many organs around the uterus (e.g., bladder, small intestine, colon, and ovaries). In addition, the size and shape of the uterus are frequently affected by the age of the patient, whereas the size and shape of the prostate are less affected by age [29]. This problem involving anatomical variation could be overcome by including more patients for training of the model.

DSC and the score of the visual evaluation were not significantly different between uteruses with and without uterine disorders, which was contrary to our expectation (i.e., automatic segmentation of uteruses with some disorders would be difficult compared to that of uteruses without the disorders). Some cases with poor segmentation were found to include small intestines, ovaries, and bladders in the automatically segmented area (Fig. 3c). To improve the accuracy of automatic segmentation of these cases, the use of MR images of various sequences might be helpful (e.g., T1-weighted and diffusion-weighted images). Small intestines and colons often exhibit high signal intensity on T1-weighted images; ovaries typically exhibit high signal intensity on diffusion-weighted images for patients of reproductive age, such that these could be easily differentiated from the uterus [30]. Another solution might be to use a 3D convolutional neural network for segmentation, as 3D anatomical information regarding the uterus could improve the accuracy of segmentation.

Our study had a few limitations. This was a small feasibility study with a retrospective design in a single institution. The performance of CNN has been shown to increase logarithmically with larger datasets [1]; thus, larger MRI datasets will likely improve the performance of automatic segmentation. In addition, the datasets included in our research were obtained with a single MR scanner vendor. To increase versatility and robustness, a multi-center and multi-scanner (i.e., multi-vendor) prospective study is desirable. Furthermore, we evaluated our model using three-fold cross-validation. Although this method could serve as an unbiased predictor, evaluation of the model using a separate test dataset would provide more objective verification. In the future, we plan to apply our model to MRI datasets obtained with various MR scanners in various institutions.

In conclusion, automatic uterine segmentation was clinically feasible with CNN, regardless of the presence of major uterine disorders. This method may be valuable for automatic detection and computer-aided diagnosis of uterine diseases in the future.

Grant support

The present study was partly supported by JSPS KAKENHI (Grant Number JP16K19883)

Conflicts of interest

None Declared.

References

[1] Y. LeCun, Y. Bengio, G. Hinton, Deep learning, Nature 521 (2015) 436–444.

[2] M.P. McBee, O.A. Awan, A.T. Colucci, C.W. Ghobadi, N. Kadom, A.P. Kansagra, S. Tridandapani, W.F. Auffermann, Deep learning in radiology, Acad. Radiol. 25 (2018) 1472–1480.

[3] R. Yamashita, M. Nishio, R.K.G. Do, K. Togashi, Convolutional Neural Networks: an Overview and Application in Radiology, Insights into Imaging, 2018.

[4] P. Lakhani, B. Sundaram, Deep learning at chest radiography: automated classification of pulmonary tuberculosis by using convolutional neural networks, Radiology 284 (2017) 574–582.

[5] K. Yasaka, H. Akai, O. Abe, S. Kiryu, Deep learning with convolutional neural network for differentiation of liver masses at dynamic contrast-enhanced CT: a preliminary study, Radiology 286 (2018) 887–896.

[6] P.F. Christ, F. Ettlinger, F. Grün, M.E.A. Elshaera, J. Lipkova, S. Schlecht, F. Ahmaddy, S. Tatavarty, M. Bickel, P. Bilic, M. Rempfler, F. Hofmann, M. D. Anastasi, S.-A. Ahmadi, G. Kaissis, J. Holch, W. Sommer, R. Braren, V. Heinemann, B. Menze, Automatic Liver and Tumor Segmentation of CT and MRI Volumes Using Cascaded Fully Convolutional Neural Networks, arXiv e-prints, 2017.

[7] R. Ha, P. Chang, S. Mutasa, J. Karcich, S. Goodman, E. Blum, K. Kalinsky, M.Z. Liu, S. Jambawalikar, Convolutional Neural Network Using a Breast MRI Tumor Dataset Can Predict Oncotype Dx Recurrence Score, J Magn Reson Imaging, 2018.

[8] Y. Song, Y.D. Zhang, X. Yan, H. Liu, M. Zhou, B. Hu, G. Yang, Computer-aided diagnosis of prostate cancer using a deep convolutional neural network from multiparametric MRI, J. Magn. Reson. Imaging 48 (2018) 1570–1577.

[9] R. Ha, P. Chang, E. Mema, S. Mutasa, J. Karcich, R.T. Wynn, M.Z. Liu, S. Jambawalikar, Fully automated convolutional neural network method for quantification of breast MRI fibroglandular tissue and background parenchymal enhancement, J. Digit. Imaging 32 (2019) 141–147.

[10] Y. Zhang, J.H. Chen, K.T. Chang, V.Y. Park, M.J. Kim, S. Chan, P. Chang, D. Chow, A. Luk, T. Kwong, M.Y. Su, Automatic Breast and Fibroglandular Tissue Segmentation in Breast MRI Using Deep Learning by a Fully-Convolutional Residual Neural Network U-Net, Academic radiology, 2019.

[11] F. Wang, Y. Wang, Y. Zhou, C. Liu, L. Xie, Z. Zhou, D. Liang, Y. Shen, Z. Yao, J. Liu, Comparison between types I and II epithelial ovarian cancer using histogram analysis of monoexponential, biexponential, and stretched-exponential diffusion models, J. Magn. Reson. Imaging 46 (2017) 1797–1809.

[12] L. Gerges, D. Popiolek, A.B. Rosenkrantz, Explorative investigation of whole-lesion histogram MRI metrics for differentiating uterine leiomyomas and leiomyosarcomas, AJR Am. J. Roentgenol. 210 (2018) 1172–1177.

[13] Y. Lakhman, H. Veeraraghavan, J. Chaim, D. Feier, D.A. Goldman, C.S. Moskowitz, S. Nougaret, R.E. Sosa, H.A. Vargas, R.A. Soslow, N.R. Abu-Rustum, H. Hricak, E. Sala, Differentiation of uterine leiomyosarcoma from atypical leiomyoma: diagnostic accuracy of qualitative MR imaging features and feasibility of texture analysis, Eur. Radiol. 27 (2017) 2903–2915.

[14] O. Ronneberger, P. Fischer, T. Brox, U-Net, Convolutional Networks for Biomedical Image Segmentation, arXiv e-prints, 2015.

[15] Y. Zhu, R. Wei, G. Gao, L. Ding, X. Zhang, X. Wang, J. Zhang, Fully Automatic Segmentation on Prostate MR Images Based on Cascaded Fully Convolution Network, J Magn Reson Imaging, 2018.

[16] F. Paugam, J. Lefeuvre, C.S. Perone, C. Gros, D.S. Reich, P. Sati, J. Cohen-Adad, Open-source Pipeline for Multi-Class Segmentation of the Spinal Cord with Deep Learning, Magn Reson Imaging, 2019.

[17] F. Shi, Q. Yang, X. Guo, T. Qureshi, Z. Tian, H. Miao, D. Dey, D. Li, Z. Fan, Vessel Wall Segmentation Using Convolutional Neural Networks, IEEE Trans Biomed Eng, 2019.

[18] B. Norman, V. Pedoia, S. Majumdar, Use of 2D U-net convolutional neural networks for automated cartilage and meniscus segmentation of knee MR imaging data to determine relaxometry and morphometry, Radiology 288 (2018) 177–185.

[19] S. Pieper, M. Halle, R. Kikinis, 3D Slicer, 2004.

[20] P. Lohmann, M. Kocher, G. Ceccon, E.K. Bauer, G. Stoffels, S. Viswanathan, M. I. Ruge, B. Neumaier, N.J. Shah, G.R. Fink, K.J. Langen, N. Galldiks, Combined FET PET/MRI radiomics differentiates radiation injury from recurrent brain metastasis, NeuroImage. Clinical 20 (2018) 537–542.

[21] F. Milletari, N. Navab, S.-A. Ahmadi, V-net, Fully Convolutional Neural Networks for Volumetric Medical Image Segmentation, 2016 Fourth International Conference on 3D Vision (3DV), IEEE, 2016, pp. 565–571.

[22] K.H. Zou, S.K. Warfield, A. Bharatha, C.M. Tempany, M.R. Kaus, S.J. Haker, W. M. Wells 3rd, F.A. Jolesz, R. Kikinis, Statistical validation of image segmentation quality based on a spatial overlap index, Acad. Radiol. 11 (2004) 178–189.

[23] J.R. Landis, G.G. Koch, The measurement of observer agreement for categorical data, Biometrics 33 (1977) 159–174.

[24] A. Fallahi, M. Pooyan, H. Ghanaati, M.A. Oghabian, H. Khotanlou, M. Shakiba, A. H. Jalali, K. Firouznia, Uterine segmentation and volume measurement in uterine fibroid patients' MRI using fuzzy C-mean algorithm and morphological operations, Iran. J. Radiol. : Q. J. Publ.Iran.Radiol. Soc. 8 (2011) 150–156.

[25] C. Militello, S. Vitabile, L. Rundo, G. Russo, M. Midiri, M.C. Gilardi, A fully automatic 2D segmentation method for uterine fibroid in MRgFUS treatment evaluation, Comput. Biol. Med. 62 (2015) 277–292.

[26] L. Rundo, C. Militello, S. Vitabile, C. Casarino, G. Russo, M. Midiri, M.C. Gilardi, Combining split-and-merge and multi-seed region growing algorithms for uterine fibroid segmentation in MRgFUS treatments, Med. Biol. Eng. Comput. 54 (2016) 1071–1084.

[27] J. Yao, D. Chen, W. Lu, A. Premkumar, Uterine Fibroid Segmentation and Volume Measurement on MRI, Medical Imaging, SPIE, 2006, p. 10.

[28] L. Rundo, C. Militello, A. Tangherloni, G. Russo, R. Lagalla, G. Mauri, M.C. Gilardi, S. Vitabile, Computer-assisted approaches for uterine fibroid segmentation in MRgFUS treatments: quantitative evaluation and clinical feasibility analysis, in: A. Esposito, M. Faundez-Zanuy, F.C. Morabito, E. Pasero (Eds.), Quantifying and Processing Biomedical and Behavioral Signals, Springer International Publishing, Cham, 2019, pp. 229–241.

[29] M. Takeuchi, K. Matsuzaki, H. Nishitani, Manifestations of the female reproductive organs on MR images: changes induced by various physiologic states, RadioGraphics 30 (2010) 1147.

[30] N. Morisawa, A. Kido, T. Koyama, T. Okada, M. Kataoka, S. Umeoka, K. Fujimoto, K. Tamai, K. Togashi, Changes of the normal ovary during menstrual cycle in reproductive age on the diffusion-weighted image, J. Comput. Assist. Tomogr. 36 (2012) 319–322.